Journal of the Serbian Society for Computational Mechanics / Vol. 3 / No. 2, 2009 / pp. 67-80

(UDC: 692.535.6:519.673)

Finite Element Modeling and Analytical Simulation of circular GLARE fiber-metal laminates subjected to lateral indentation

G. J. Tsamasphyros[1] and G. S. Bikakis[1*]

[1]National Technical University of Athens, Strength of Materials Laboratory, 9 Iroon Polytechniou, Zographou, GR 157 73, Athens, Greece
trixaton@central.ntua.gr
**Corresponding author*

Abstract

GLARE is a Fiber-Metal Laminated material used in aerospace structures which are frequently subjected to various impact damages. Hence, response of GLARE plates subjected to lateral indentation is very important. No FEM or other analytical solution of this problem is known to the authors.

This paper deals with the static response of thin circular clamped GLARE plates under the action of a lateral hemispherical indentor located at their center. We propose a finite element modeling procedure for the calculation of static load-indentation curve and the first failure load and deflection due to glass-epoxy tensile fracture applicable to GLARE plates. Additionally, we further verify the validity of the analytical model for the solution of this problem which we have derived using the Ritz method in our previous work.

A 3-D solid modeling procedure with ANSYS is implemented. We employ an isotropic non-linear elastoplastic material model which obeys a true stress-strain relation for aluminum. An orthotropic linear elastic material model is used for the glass-epoxy. The contact between the indentor and the plate is simulated by contact elements. We use non-linear analysis with geometric and material non-linearities. The indentor is forced to move and deform the plate incrementally. Analysis stops when first failure due to glass-epoxy tensile fracture occurs. This FEM procedure and our analytical model are applied to GLARE 2-2/1-0.3 and to GLARE 3-3/2-0.4 plates with various diameters.

We compare FEM results with analytical results and their good agreement is demonstrated. Furthermore, FEM and analytical results are compared with published experimental data for the case of a GLARE 2-2/1-0.3 plate with a radius of 40 mm. Both numerical and analytical load-indentation curves and first failures agree well with the experimental values (failure load within 2% and 7%, failure deflection within 5% and 3% respectively).

It is shown that our analytical results converge satisfactorily. Also, the expected governing role of the membrane in comparison with the bending stiffness is demonstrated. Finally, FEM plots of lateral GLARE plate deflections justify the axisymmetrical deflection shape considered by the authors.

Keywords: GLARE, laminate, indentation, fracture, FEM

1. Introduction

This paper focuses on the response of thin circular clamped GLARE fiber-metal laminated plates which are subjected to lateral indentation. Among other applications, GLARE is mainly used in aerospace structures and has higher impact resistance in comparison with conventional composites or aluminum alloys (Vogelesang and Vlot 2000, Vermeeren 2003).

Impact properties are very important in aerospace structures, since impact damage is caused by various sources, such as maintenance damage from dropped tools, collision between service cars or cargo and the structure, bird strikes and hail (Vogelesang and Vlot 2000, Vermeeren 2003, Vlot 1996, Vlot 1993, Laliberte et al. 2002). A large amount of the energy absorbed by GLARE plates during low velocity, high velocity or even ballistic impacts is due to the static deformation of the plate (Vlot 1996, Hoo Fat et al. 2003, Lin and Hoo Fat 2006). In this regard, the response of GLARE plates subjected to lateral indentation is very important as far as their overall impact behavior is concerned.

In this work we deal with the static response of thin circular clamped GLARE fiber-metal laminated plates under the action of a lateral hemispherical indentor located at the center of the plate. Vlot (1996) used an elastic-plastic impact model to solve this problem numerically assuming a deformation profile based on experimental data. Hoo Fatt et al. (2003) used the principle of minimum potential energy to model analytically the response of fully clamped square GLARE panels assuming a deformation profile which resembles that of a stretched membrane. They also calculated the first failure load due to glass-epoxy tensile fracture. In our previous work (2008), we employed the Ritz method and derived formulas corresponding to one, two and three-parameter approximation functions for the calculation of lateral indentation response applicable to thin circular GLARE plates.

The first objective of this paper is to develop a finite element modeling procedure for the calculation of static load-indentation curve and the first failure load and deflection due to glass-epoxy tensile fracture of thin circular clamped GLARE fiber-metal laminated plates under the action of a lateral hemispherical indentor located at their center. The ANSYS finite element program is used for this purpose. The second objective is to verify the validity of our analytical model (2008) by application to GLARE 2-2/1-0.3 and to GLARE 3-3/2-0.4 circular plates with various diameters and by comparison of analytical results with the corresponding FEM results.

We compare numerical results with analytical results and their good agreement is demonstrated. Furthermore, FEM and analytical results agree well with published experimental data for the case of a GLARE 2-2/1-0.3 plate with a radius of 40 mm (Vlot 1996). No FEM or other analytical solution of this problem is known to the authors.

In the following sections the definition of the problem is first given, then details of the FEM modeling and analytical simulation are presented followed by the obtained results and the final conclusions.

2. Problem definition

We consider a thin clamped circular GLARE plate with radius α and thickness t as shown in Fig. 1. The plate is loaded statically by an indentor with a hemispherical tip of radius R acting at the center. The plate consists of alternating layers of aluminum and glass-epoxy. The aspect ratio α/t is assumed very high so that shear deformation and local indentation are negligible.

A polar coordinate system (r, θ, z) with the origin at the center of the plate is employed for the analytical formulation as illustrated in Fig. 1 The plate is considered clamped along its

boundary. As the indentor progresses the load P applied on the plate and the corresponding central deflection w_o increase. The (P , w_o) curve and the first failure load and deflection due to glass-epoxy tensile fracture will be calculated analytically and numerically using ANSYS.

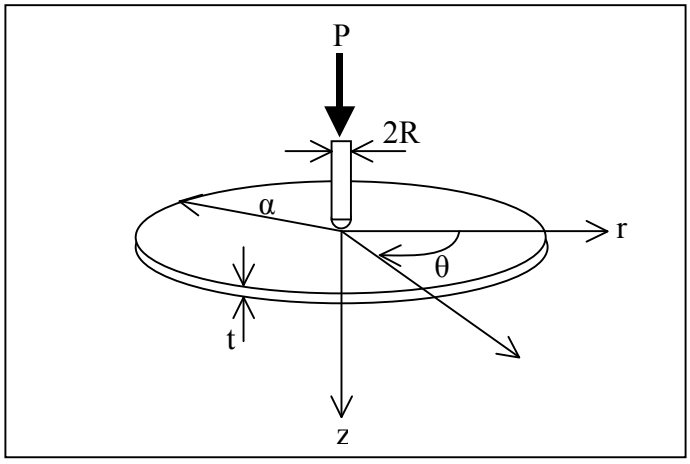

Fig. 1. Circular plate problem geometry and coordinate system

3. Finite element modeling

In this paper we implement a finite element modeling procedure to predict the static response of thin circular clamped GLARE fiber-metal laminated plates under the action of a lateral hemispherical indentor located at the center of the plate. ANSYS finite element program is used for this purpose.

The GLARE plate is modeled with two solid elements of different type along its thickness. The external aluminum layer, which is in contact with the indentor, is modeled with SOLID 185 elements. These hexahedral-shaped elements have eight nodes with three translational degrees of freedom per node. In order to reduce the computational cost, the remaining layers of the GLARE plate are modeled with SOLSH 190 elements. These are also hexahedral-shaped layered elements with eight nodes and three translational degrees of freedom per node. The accuracy of these elements is governed by the first order shear deformation theory.

The indentor is also modeled with SOLID 185 elements. In order to simulate the contact between the indentor and the external surface of the GLARE plate, we use CONTA 174 and TARGE 170 elements in way of the contact areas. The plate is clamped along its boundary. Due to symmetry of the problem we further reduce the computational cost by modeling only one quarter of the structure. Suitable symmetry boundary conditions are applied in this regard to all nodes of the symmetry planes.

The material of the steel indentor, which is considered rigid, is modeled with an isotropic linear elastic material model with increased stiffness. We idealize the material behavior of the GLARE plate unidirectional glass-epoxy layers by employing an orthotropic linear elastic material model. The material of the GLARE plate 2024-T3 aluminum layers is modeled with an

isotropic non-linear elastoplastic material model which obeys the following true stress-strain relation (Chandrakanth and Pandey 1998):

$$\sigma = \sigma_O + \kappa \varepsilon^{\frac{1}{n}} \tag{1}$$

where σ_O is the yield stress of 2024-T3 aluminum, $\kappa = 650$ and $n = 1.62$.

A static non-linear analysis is employed with geometric and material non-linearities. The indentor is forced to move and deform the GLARE plate incrementally. Our analysis stops when the first failure due to glass-epoxy tensile fracture occurs. The maximum tensile strain criterion is used in order to verify when first failure occurs. The corresponding indentor's position and load are then recorded as the first failure deflection and load.

In order to verify the convergence of FEM results, (P , w_o) curve and the first failure load and deflection due to glass-epoxy tensile fracture, we built three models with increasing plate mesh density for each specific case of circular GLARE plate we analyze. A fine mesh is used for the indentor in order to represent its geometry accurately. The indentor's mesh density remains the same for all models. A typical fine mesh of a GLARE plate along with the indentor is depicted in Fig. 2.

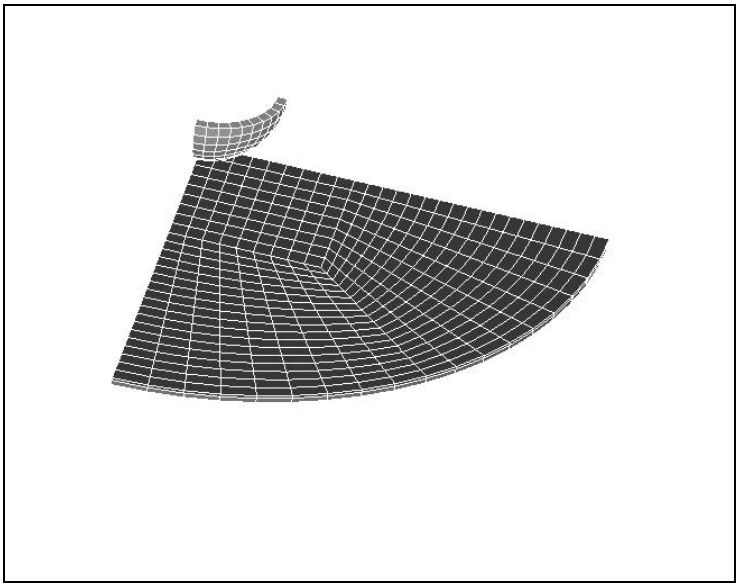

Fig. 2. Finite element mesh of a GLARE 2 plate with the indentor

We apply this finite element modeling procedure to GLARE 2-2/1-0.3 circular plates with 35 mm, 40 mm and 45 mm radius and to GLARE 3-3/2-0.4 circular plates with 65 mm, 70 mm and 75 mm radius. A total of eighteen finite element models have been implemented. The numerical results are compared with the corresponding analytical results and published experimental data for the case of a GLARE 2-2/1-0.3 plate with a radius of 40 mm (Vlot 1996).

4. Analytical simulation

We previously derived (2008) analytical formulas corresponding to one, two and three-parameter Ritz approximations of the deformation profile for the calculation of static load-indentation curve and first failure load and deflection due to glass-epoxy tensile fracture applicable to thin circular clamped GLARE fiber-metal laminated plates under the action of a lateral hemispherical indentor located at their center. Two cases of plate stiffness were considered. Firstly, due to very large deflections, the bending resistance is neglected and only the membrane resistance of the plate is taken into account. In the second case, both bending and membrane resistance are taken into account. The derived formulas were applied to a GLARE 2-2/1-0.3 plate with 40 mm radius. In this work, in order to verify the validity of our analytical solution, we apply the derived formulas to GLARE 2-2/1-0.3 circular plates with 35 mm and 45 mm radius and to GLARE 3-3/2-0.4 circular plates with 65 mm, 70 mm and 75 mm radius. The analytical results are compared with the corresponding FEM results and available published experimental data for the case of a GLARE 2-2/1-0.3 plate with a radius of 40 mm (Vlot 1996). In the following paragraph a short presentation of the analytical equations for the solution of the circular GLARE plate indentation problem is given from Tsamasphyros and Bikakis (2008).

4.1 Analytical equations

For one Ritz parameter, considering both bending and membrane plate resistance, the indentation load is directly calculated by the following equation:

$$P = \left[0.576\left(N_x + N_y\right) + 0.734N_{xy}\right]w_o + \left[0.62\left(A_{11} + A_{22}\right) + 0.412\left(A_{12} + 2A_{66}\right)\right]\frac{w_o^3}{\alpha^2} + 4M_{xy} +$$

$$+\left[\left(3.318 + 2.906\ln\alpha\right)\left(D_{11} + D_{22}\right) + \left(-8.124 + 1.938\ln\alpha\right)D_{12} + \left(14.758 + 3.876\ln\alpha\right)D_{66}\right]\frac{w_o}{\alpha^2} \tag{2}$$

N_x, N_y and N_{xy} are the in-plane forces of the aluminum layers calculated as follows:

$$N_x = N_y = m\sigma_o t_{Al},$$

$$N_{xy} = m\frac{\sigma_o}{\sqrt{3}}t_{Al} \tag{3}$$

where m is the number of aluminum layers and t_{Al} is the thickness of each aluminum layer.

A_{ij} and D_{ij} are the extensional and bending stiffnesses of the laminate. M_{xy} is the twisting moment acting on the aluminum layers calculated as follows (for $m = 1$ or $m = 2,4,...$ or $m = 3,5,...$ respectively in equation 4):

$$M_{xy} = \sigma_o\frac{t_{Al}^2}{4\sqrt{3}},$$

$$M_{xy} = \frac{\sigma_o t_{Al}}{\sqrt{3}}\sum_{i=1}^{m} Z_i,$$

$$M_{xy} = \frac{\sigma_o t_{Al}}{\sqrt{3}}\sum_{i=1}^{m-1} Z_i + \sigma_o\frac{t_{Al}^2}{4\sqrt{3}} \tag{4}$$

where Z_i is the geometric distance of each aluminum layer from the neutral surface of the plate.

For one Ritz parameter, considering only the membrane plate resistance, P is calculated from equation (2) where M_{xy} and all D_{ij} terms are now equal to zero.

For two Ritz parameters, considering both bending and membrane plate resistance, the solution of the following (2x2) non-linear system of algebraic equations yields the unknown Ritz coefficients λ_1 and λ_2 for specific values of load P (w_o is obtained by adding λ_1 and λ_2):

$$P = 2N_1\lambda_1 - N_3\lambda_2 + 4M_1\lambda_1^3 - M_5\lambda_2^3 + 2M_3\lambda_1\lambda_2^2 - 3M_4\lambda_1^2\lambda_2 + 4M_{xy} + 2C_1\lambda_1 + C_3\lambda_2 \tag{5}$$

$$P = -N_3\lambda_1 + 2N_2\lambda_2 - M_4\lambda_1^3 + 4M_2\lambda_2^3 - 3M_5\lambda_1\lambda_2^2 + 2M_3\lambda_1^2\lambda_2 + 4M_{xy} + 2C_2\lambda_2 + C_3\lambda_1 \tag{6}$$

where:

$$N_1 = 0.288(N_x + N_y) + 0.367N_{xy},$$

$$N_2 = 11.916(N_x + N_y) + 15.171N_{xy} \tag{7}$$

$$N_3 = 0.218(N_x + N_y) + 0.278N_{xy},$$

$$M_1 = \left[0.155(A_{11} + A_{22}) + 0.103\left(A_{12} + 2A_{66}\right)\right]\frac{1}{\alpha^2} \tag{8}$$

$$M_2 = \left[205.585(A_{11} + A_{22}) + 137.056\left(A_{12} + 2A_{66}\right)\right]\frac{1}{\alpha^2} \tag{9}$$

$$M_3 = \left[19.449(A_{11} + A_{22}) + 12.966\left(A_{12} + 2A_{66}\right)\right]\frac{1}{\alpha^2} \tag{10}$$

$$M_4 = \left[1.211(A_{11} + A_{22}) + 0.807\left(A_{12} + 2A_{66}\right)\right]\frac{1}{\alpha^2},$$

$$M_5 = \left[8.033(A_{11} + A_{22}) + 5.356\left(A_{12} + 2A_{66}\right)\right]\frac{1}{\alpha^2} \tag{11}$$

$$C_1 = \left[(1.659 + 1.453\ln\alpha)(D_{11} + D_{22}) + (-4.062 + 0.969\ln\alpha)D_{12} + (7.379 + 1.938\ln\alpha)D_{66}\right]\frac{1}{\alpha^2} \tag{12}$$

$$C_2 = \left[(1114.758 + 36.335\ln\alpha)(D_{11} + D_{22}) + (613.985 + 24.224\ln\alpha)D_{12} + (1615.549 + 48.447\ln\alpha)D_{66}\right]\frac{1}{\alpha^2} \tag{13}$$

$$C_3 = \left[-5.826\left(D_{11} + D_{22}\right) - 55.56D_{12} + 43.908D_{66}\right]\frac{1}{\alpha^2} \tag{14}$$

For two Ritz parameters, considering only the membrane plate resistance, the unknown Ritz coefficients are calculated from equations (5) and (6) where M_{xy} and all C_i terms are now equal to zero.

For three Ritz parameters, considering both bending and membrane plate resistance, the solution of the following (3x3) non-linear system of algebraic equations yields the unknown Ritz coefficients λ_1, λ_2 and λ_3 for specific values of load P (w_o is obtained by adding λ_1 , λ_2 and λ_3):

$$P = 2N_1\lambda_1 - N_3\lambda_2 - N_6\lambda_3 + 4M_1\lambda_1^3 - M_5\lambda_2^3 - M_{11}\lambda_3^3 + 2M_3\lambda_1\lambda_2^2 - 3M_4\lambda_1^2\lambda_2 +$$

$$+ 2M_7\lambda_1\lambda_3^2 - 3M_{12}\lambda_1^2\lambda_3 - M_{15}\lambda_2\lambda_3^2 + M_{13}\lambda_2^2\lambda_3 - 2M_{14}\lambda_1\lambda_2\lambda_3 + 4M_{xy} + 2C_1\lambda_1 + C_3\lambda_2 + C_6\lambda_3 \tag{15}$$

$$P = -N_3\lambda_1 + 2N_2\lambda_2 - N_5\lambda_3 - M_4\lambda_1^3 + 4M_2\lambda_2^3 - M_{10}\lambda_3^3 - 3M_5\lambda_1\lambda_2^2 + 2M_3\lambda_1^2\lambda_2 -$$

$$- M_{15}\lambda_1\lambda_3^2 - M_{14}\lambda_1^2\lambda_3 + 2M_8\lambda_2\lambda_3^2 - 3M_9\lambda_2^2\lambda_3 + 2M_{13}\lambda_1\lambda_2\lambda_3 + 4M_{xy} + C_3\lambda_1 + 2C_2\lambda_2 + C_5\lambda_3 \tag{16}$$

$$P = -N_6\lambda_1 - N_5\lambda_2 + 2N_4\lambda_3 - M_{12}\lambda_1^3 - M_9\lambda_2^3 + 4M_6\lambda_3^3 + M_{13}\lambda_1\lambda_2^2 - M_{14}\lambda_1^2\lambda_2 -$$

$$-3M_{11}\lambda_1\lambda_3^2 + 2M_7\lambda_1^2\lambda_3 - 3M_{10}\lambda_2\lambda_3^2 + 2M_8\lambda_2^2\lambda_3 - 2M_{15}\lambda_1\lambda_2\lambda_3 + 4M_{xy} + C_6\lambda_1 + C_5\lambda_2 + 2C_4\lambda_3 \quad (17)$$

where:

$$N_4 = 39.046(N_x + N_y) + 49.715N_{xy},\ N_5 = 0.361(N_x + N_y) + 0.459N_{xy} \quad (18)$$

$$N_6 = 0.141(N_x + N_y) + 0.18N_{xy},\ M_6 = \left[2191.104(A_{11} + A_{22}) + 1460.737\left(A_{12} + 2A_{66}\right)\right]\frac{1}{\alpha^2} \quad (19)$$

$$M_7 = \left[64.237(A_{11} + A_{22}) + 42.825\left(A_{12} + 2A_{66}\right)\right]\frac{1}{\alpha^2} \quad (20)$$

$$M_8 = \left[2665.467(A_{11} + A_{22}) + 1776.976\left(A_{12} + 2A_{66}\right)\right]\frac{1}{\alpha^2} \quad (21)$$

$$M_9 = \left[35.223(A_{11} + A_{22}) + 23.482\left(A_{12} + 2A_{66}\right)\right]\frac{1}{\alpha^2} \quad (22)$$

$$M_{10} = \left[46.016(A_{11} + A_{22}) + 30.678\left(A_{12} + 2A_{66}\right)\right]\frac{1}{\alpha^2} \quad (23)$$

$$M_{11} = \left[16.677(A_{11} + A_{22}) + 11.118\left(A_{12} + 2A_{66}\right)\right]\frac{1}{\alpha^2} \quad (24)$$

$$M_{12} = \left[0.378(A_{11} + A_{22}) + 0.252\left(A_{12} + 2A_{66}\right)\right]\frac{1}{\alpha^2} \quad (25)$$

$$M_{13} = \left[168.625(A_{11} + A_{22}) + 112.416\left(A_{12} + 2A_{66}\right)\right]\frac{1}{\alpha^2} \quad (26)$$

$$M_{14} = \left[28.253(A_{11} + A_{22}) + 18.835\left(A_{12} + 2A_{66}\right)\right]\frac{1}{\alpha^2} \quad (27)$$

$$M_{15} = \left[55.382(A_{11} + A_{22}) + 36.921\left(A_{12} + 2A_{66}\right)\right]\frac{1}{\alpha^2} \quad (28)$$

$$C_4 = \left[(11744.949 + 117.727\ln\alpha)(D_{11} + D_{22}) + (7411.381 + 78.485\ln\alpha)D_{12} + \right.$$

$$\left. + (16078.518 + 156.97\ln\alpha)D_{66}\right]\frac{1}{\alpha^2} \quad (29)$$

$$C_5 = \left[-29.824\left(D_{11} + D_{22}\right) - 484.976D_{12} + 425.329D_{66}\right]\frac{1}{\alpha^2} \quad (30)$$

$$C_6 = \left[-12.788\left(D_{11} + D_{22}\right) - 101.545D_{12} + 75.967D_{66}\right]\frac{1}{\alpha^2} \quad (31)$$

For three Ritz parameters, considering only the membrane plate resistance, the unknown Ritz coefficients are calculated from equations (15), (16) and (17) where M_{xy} and all C_i terms are now equal to zero.

First failure due to glass-epoxy tensile fracture occurs when:

$$\sum_{j=1}^{i} \lambda_j (4j-3) = \frac{2\alpha}{\pi}\sqrt{2\varepsilon_{crit}}\,, \qquad i = 1,2,3,... \tag{32}$$

where ε_{crit} is the tensile failure strain of the glass-epoxy.

Depending on the number of Ritz parameters, and considering the case of membrane only resistance or the case of both bending and membrane resistance, we use the appropriate set of the aforementioned equations. We start increasing the indentation load P, until the corresponding values of λ_j satisfy condition (32). When this happens, the indentation load P has reached the critical value P_{crit} and the corresponding first failure displacement w_{ocrit} is then calculated, for those λ_j values, from the following equation:

$$w_o = \sum_{j=1}^{i} \lambda_j\,, \qquad i = 1,2,3,... \tag{33}$$

5. Results

We have applied the proposed finite element modeling procedure and the analytical formulas to GLARE 2-2/1-0.3 plates and to GLARE 3-3/2-0.4 plates. GLARE 2-2/1-0.3 fiber-metal laminate consists of two external 2024-T3 aluminum layers and two R-glass UD fiber prepregs in the middle. Each aluminum layer has a thickness of 0.3mm and each prepreg has a thickness of 0.1 mm. Prepregs have the same orientation. We have analyzed circular GLARE 2 plates with 35 mm, 40 mm and 45 mm radius. The material properties considered for our calculations are given in Table 1. All available properties of reference (Vlot 1996) have been used. For 2024-T3 aluminum we have considered a Poisson's ratio equal to 0.33 (Alderliesten 2005). Remaining material properties have been taken from Hoo Fat et al. (2003) or have been calculated based on the reciprocal relations.

$E_{11} = 47.3\ GPa$ (long. prepreg stiffness)	$\nu_{12} = 0.25$ (prepreg Poisson's ratio)
$E_{22} = 17\ GPa$ (trans. prepreg stiffness)	$\nu_{13} = 0.25$ (prepreg Poisson's ratio)
$E_{33} = 17\ GPa$ (through thickness stiffness)	$\nu_{23} = 0.32$ (prepreg Poisson's ratio)
$G_{12} = 7$ GPa (in-plane shear modulus)	$\varepsilon_{crit} = 0.055$ (prepreg tensile failure strain)
$G_{13} = 7$ GPa (out-of-plane shear modulus)	$E_{Al} = 72\ GPa$(aluminum Young modulus)
$G_{23} = 7$ GPa (out-of-plane shear modulus)	$\sigma_o = 340\ MPa$ (aluminum yield strength)
	$\nu_{Al} = 0.33$ (aluminum Poisson's ratio)

Table 1. GLARE 2-2/1-0.3 material properties

GLARE 3-3/2-0.4 fiber-metal laminate consists of the following lay-up:

[2024-T3 / 0^0 glass / 90^0 glass / 2024-T3 / 90^0 glass / 0^0 glass / 2024-T3]

Each 2024-T3 aluminum layer has a thickness of 0.4 mm. Each prepreg ply has a thickness of 0.125 mm and consists of S2-glass UD fiber prepregs. We have analyzed circular GLARE 3 plates with 65 mm, 70 mm and 75 mm radius. The material properties considered for our

calculations are those given in Table 1, apart from ε_{crit} which, according to our correspondence with the manufacturer of GLARE 3, is equal to 0.047.

The finite element modeling results and analytical simulation results are presented and compared in the following paragraphs.

5.1 Finite element modeling results

In Fig. 3 the lateral deflections of a GLARE 2-2/1-0.3 circular plate under the action of the indentor are illustrated. This is a representative deflection plot for the two different GLARE grades we examine. An axisymmetrical deflection shape can be observed. This observation further enhances Vlot's experimental results (1996) concerning the axisymmetrical deflection shape of GLARE plates, which has been considered by Vlot for his elastic - plastic impact model. It is noted that we have also considered an axisymmetrical deflection shape for our analytical simulation (2008). In Fig. 4 a representative deformed shape of a GLARE plate is depicted. For these plots we have used ANSYS symmetry expansion command in order to obtain results corresponding to a full model, since we have modeled a quarter of the structure. In Fig. 5 the static (P , w_o) curves of a circular GLARE 2-2/1-0.3 plate with a radius of 40 mm are depicted.

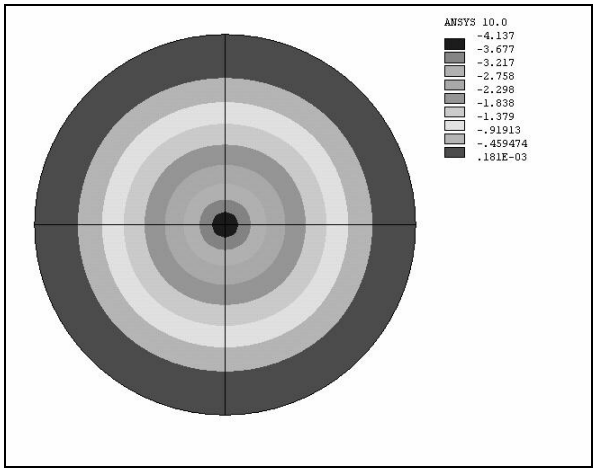

Fig. 3. Lateral deflections in mm of a GLARE 2 plate with 40 mm radius and 4.137 mm indentation

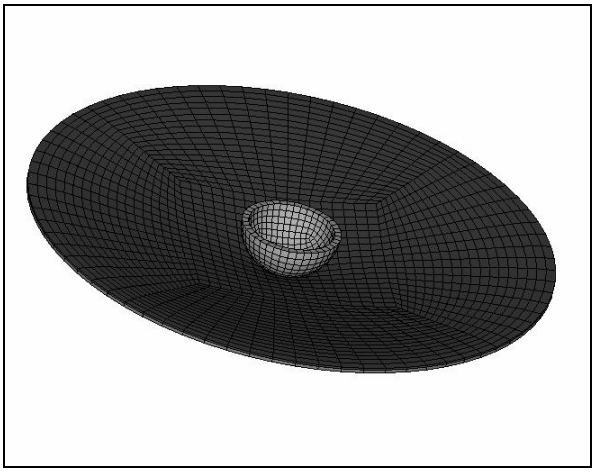

Fig. 4. Deformed shape of GLARE 2 plate with 40 mm radius

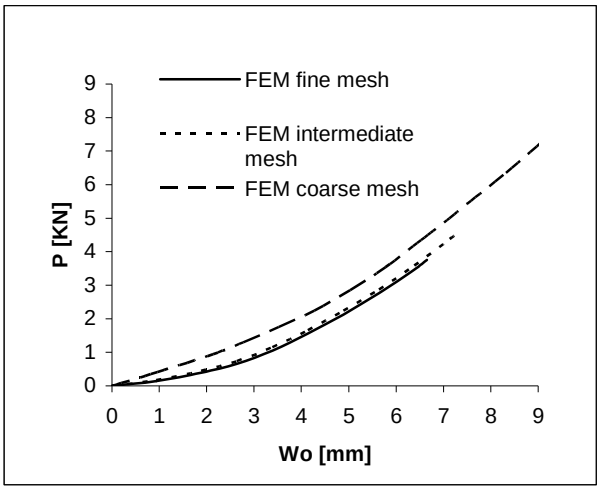

Fig. 5. Load-indentation curves for GLARE 2 plate with 40 mm radius

Apart from the (P , w_o) curve which corresponds to the coarse mesh, all other depicted curves stop at the point of the predicted first failure. It can be seen that the results converge satisfactorily. Similar behavior has been found in the cases of GLARE 2-2/1-0.3 plates with 35 mm, 45 mm radius and GLARE 3-3/2-0.4 plates with 65 mm, 70 mm, 75 mm radius.

5.2 Analytical simulation results

In Fig. 6 the static (P , w_o) curves corresponding to the membrane strain energy of circular GLARE 2-2/1-0.3 plate with a radius of 40 mm are depicted. In Fig. 7 the static (P , w_o) curves corresponding to both bending and membrane strain energy of the same GLARE 2 plate are depicted.

Each analytical depicted curve stops at the point of the predicted first failure. It can be seen that the results converge satisfactorily in both examined cases.

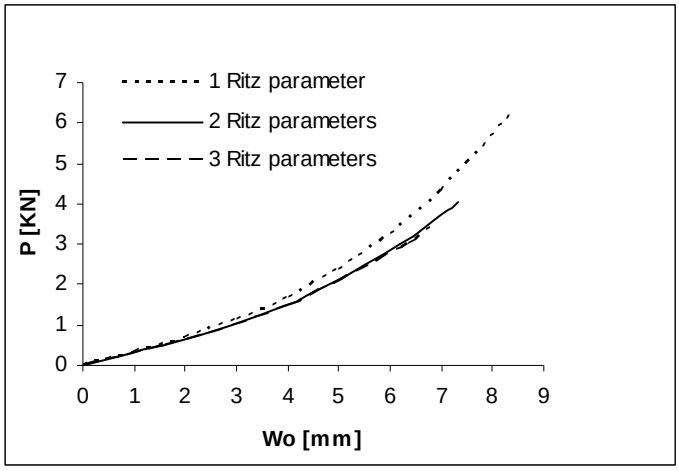

Fig. 6. Membrane Load-indentation curves for GLARE 2 plate with 40 mm radius

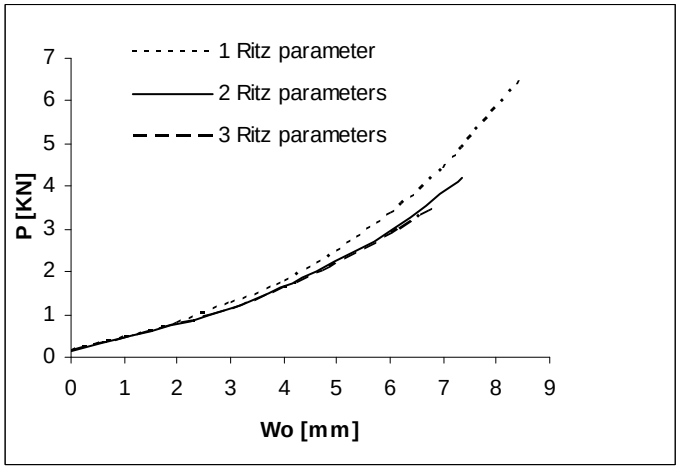

Fig. 7. Membrane & Bending Load-indentation curves, GLARE 2 plate, 40 mm radius

It is noted that the rigid-perfectly plastic assumption for the aluminum yields the existence of constant bending terms in (P , w_o) expressions. Due to these terms the plate does not deflect until the load reaches a finite value that causes plastic flow. This is clearly illustrated in Fig. 7.

Similar behavior has been found in the cases of GLARE 2-2/1-0.3 plates with 35 mm, 45 mm radius and GLARE 3-3/2-0.4 plates with 65 mm, 70 mm, 75 mm radius.

5.3 Comparison of FEM, analytical and experimental results

In Fig. 8 the static three - parameter (P , w_o) curves corresponding to the membrane strain only and to both bending and membrane strain energy are compared with the fine mesh FEM (P , w_o) curve. A good agreement between numerical and analytical results is

demonstrated. The expected (Tsamasphyros and Bikakis 2008) small contribution of bending stiffness in comparison with the membrane stiffness to the response of the GLARE plates can be observed from the analytical curves. A good agreement between numerical and analytical results and the small contribution of bending stiffness in comparison with the membrane stiffness has also been found in the cases of GLARE 2-2/1-0.3 plates with 35 mm, 45 mm radius and GLARE 3-3/2-0.4 plates with 65 mm, 70 mm, 75 mm radius.

Furthermore, both numerical and analytical results are compared with the experimental (P , w_o) curve published by Vlot (1996) for the case of a GLARE 2-2/1-0.3 circular plate with a radius of 40 mm. A good agreement between calculations and experimental data is found. The best numerical prediction, corresponding to the fine mesh FEM results, yields a first failure load of 3.75 KN and a first failure deflection of 6.65 mm which are within 2% and within 5% of the corresponding experimental values (3.8 KN and 7mm). The best analytical prediction, corresponding to the three - parameter Ritz approximation that takes into account both bending and membrane stiffness of the plate, yields a first failure load of 3.57 KN and a first failure deflection of 6.85 mm which are within 7% and within 3% of the corresponding experimental values.

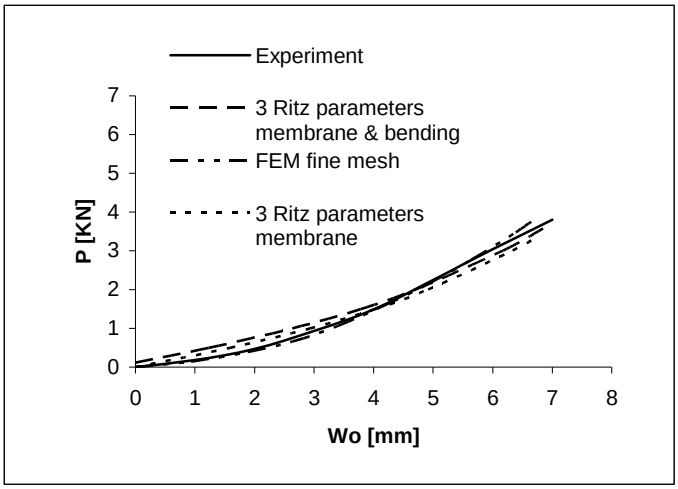

Fig. 8. Experimental vs. calculated Load-indentation curves, GLARE 2 plate, 40 mm radius

6. Conclusions

In this work we have developed a finite element modeling procedure for the prediction of the static load-indentation curve of thin circular clamped GLARE fiber-metal laminated plates that deflect under the action of a lateral hemispherical indentor located at their center. ANSYS finite element program is used for this purpose. The modeling procedure also predicts the first failure load and deflection due to glass-epoxy tensile fracture.

We have applied the finite element modeling procedure along with our analytical model (2008) to predict the response of circular GLARE 2-2/1-0.3 plates with 35 mm, 40 mm and 45 mm radius and circular GLARE 3-3/2-0.4 plates with 65 mm, 70 mm and 75 mm radius. The numerical results are compared with corresponding analytical results. Both numerical and analytical results are compared with published experimental data from reference (Vlot 1996).

It is found that both numerical and analytical results have converged satisfactorily. The governing role of the membrane in comparison with the bending stiffness for this problem is demonstrated by comparison between membrane only three-parameter Ritz approximation results and both bending and membrane three-parameter Ritz approximation results. Both numerically and analytically predicted load-indentation curves for a GLARE 2-2/1-0.3 circular plate with a radius of 40 mm agree well with the corresponding experimental curve (Vlot 1996). Also, the numerically calculated first failure load and deflection are within 2% and 5% of their experimental values respectively, while the analytically calculated first failure load and deflection are within 7% and 3% of their experimental values respectively. As expected, the FEM load-indentation curve fits better with the experimental data than the analytical curves.

The analytical load-indentation curves are also in good agreement with the corresponding numerical curves in all other examined cases. There is also a good agreement between analytically and numerically predicted first failure load and deflection. In this regard, the validity of our analytical model is verified.

Fine mesh plots of FEM results concerning the lateral deflections of all examined GLARE plates under lateral indentation, for all intermediate positions of the indentor, justify the axisymmetrical deflection shape considered by Vlot (1996) and for our analytical model.

By careful examination of all results we have obtained, it is concluded that the (P , w_o) curve of a GLARE plate under lateral indentation can be approximated up to the point of first failure, considering only one Ritz parameter and only the membrane components of the strain energy. This conclusion is very useful in cases where the prediction of first failure is not mandatory, since it reduces the required calculations dramatically.

The proposed finite element modeling procedure and our analytical simulation model can be used for the design of circular GLARE plates under lateral indentation and for the evaluation of the impact properties of different GLARE grades. Furthermore, our analytical simulation model is expected to predict satisfactorily the lateral indentation response of thin circular plates consisting of other advanced hybrid material systems of alternating metal layers bonded to fiber-reinforced polymer layers, provided that our assumptions remain valid.

Also, the proposed finite element modeling procedure is expected to predict satisfactorily the lateral indentation response of thin GLARE plates with various geometries and boundary conditions, under the action of hemispherical indentors with arbitrary position upon the plate. Finally, this finite element modeling procedure is expected to predict satisfactorily the lateral indentation response of thin plates consisting of other advanced hybrid material systems of alternating metal layers bonded to fiber-reinforced polymer layers, provided that a suitable material model is employed for the metal layers.

References

Alderliesten R (2005). Fatigue crack propagation and delamination growth in GLARE. Delft University Press, Delft, The Netherlands.

Chandrakanth S, Pandey PC (1998). Damage coupled elasto-plastic finite elementanalysis of a Timoshenko layered beam, *Computers and Structures*, 69, 411-420.

Hoo Fatt MS, Lin C, Revilock Jr DM, Hopkins DA (2003). Ballistic impact of GLARE^{TM} fiber-metal laminates, *Composite Structures*, 61/1-2, 73-88.

Laliberte JF, Poon C, Straznicky PV, Fahr A (2002). Post-impact fatigue damage growth in fiber-metal laminates, *International Journal of Fatigue*, 24, 249-255.

Lin C, Hoo Fatt MS (2006). Perforation of composite plates and sandwich panels under quasi-static and projectile loading, *Journal of Composite Materials*, 40/20, 1801-1840.

Tsamasphyros GJ, Bikakis GS (2008). Response of Circular GLARE Fiber – Metal Laminates under Lateral Indentation. Proc. Ninth International Conference on Computational Structures Technology (CST 2008) (Eds. B.H.V. Topping and M. Papadrakakis), Athens, Greece.

Vermeeren CAJR (2003). An historic overview of the development of fibre metal laminates, *Applied Composite Materials*, 10, 189-205.

Vlot A (1996). Impact loading on fibre metal laminates, *International Journal of Impact Engineering*, 18/3, 291-307.

Vlot A (1993). Impact properties of fibre metal laminates, *Composites Engineering*, 3/10, 911-927.

Vogelesang LB, Vlot A (2000). Development of fibre metal laminates for advanced aerospace structures, *Journal of Materials Processing Technology*, 103, 1-5